The Significance of Accurate Needle Electrode Geometry Definitions in Discharge Plasma Finite-Element Simulations: A Comparative Analysis

Mohammad Hamidieh, *Student Member*, *IEEE*, and Mona Ghassemi, *Senior Member*, *IEEE*Zero Emission, Realization of Optimized Energy Systems (ZEROES) Laboratory

Department of Electrical and Computer Engineering, The University of Texas at Dallas, Richardson, TX, USA mohammad.hamidieh@utdallas.edu, mona.ghassemi@utdallas.edu

Abstract- This paper aims to explore the significance of accurately defining the geometry of needle electrodes in gas discharge plasma finite-element simulations and evaluate the sensitivity and responsiveness of simulation outputs to different needle electrode shapes. Using a hydrodynamic (drift-diffusion) model and COMSOL Multiphysics software, a comprehensive numerical analysis is performed to investigate the influence of six needle geometries (hyperbolic, elliptic, and circle-with-tangents) with an equal radius of curvature on negative air discharge plasma characteristics. The study aims to establish a comparative understanding of how the defined geometries relate to the behavior of the discharge plasma. Various aspects, including the properties of Trichel pulses, the spatiotemporal evolution of charged species, and the electrical field distribution, are explored.

I. INTRODUCTION

The complex nature of gas discharge plasmas coupled with the challenges posed by experimental investigations necessitates the utilization of advanced computational tools to deepen our understanding of their underlying mechanisms. Finite-element simulations, in particular, have emerged as a popular approach, offering a powerful tool to model and analyze discharge plasmas. This capability empowers researchers to optimize novel designs for both technological applications utilizing plasma and the development of reliable insulation systems for high-voltage power system components. Noteworthy examples are more- or all-electric aircraft and allelectric ships where the incorporation of high power density and high voltage concepts introduces elevated levels of electric stress and temperatures in harsh conditions of cruising altitudes. Consequently, the development of innovative designs becomes imperative to achieve compact, cost-effective, and dependable insulation systems [1-10].

In this paper, our primary objective is to investigate the sensitivity of non-thermal, non-equilibrium gas discharge plasmas to the defined geometry within the framework of finite-element simulations. Needle-plane electrode systems are one of the well-studied geometry because they can characterize real-world electrode systems featuring sharp conductors in front of conducting flat objects. However, a critical question remains: to what extent are the simulation outputs of gas discharge plasmas influenced by the shape of the needle electrode? In other words, how crucial is it to accurately specify the exact needle geometry for the simulations? This paper addresses this

question by presenting an in-depth comparative analysis of the initiation and propagation of negative air discharges under varying needle shapes. When a sharp electrode is subjected to a negative DC voltage exceeding the corona onset level, a pulsating current emerges in the external circuit (interelectrode gap), known as Trichel pulses. Over time, both experimental and simulation techniques [11-20] have become widely utilized in the study of negative discharges and Trichel pulses, describing their physical and chemical complexities. By employing the hydrodynamic (drift-diffusion) model and COMSOL Multiphysics software, we intend to analytically and numerically investigate the intricate interplay between defined geometry and negative air discharge plasma behavior. This paper explores various spatiotemporal aspects of this behavior, such as discharge current patterns, charged species evolution, and electrical field distribution.

II. HYDRODYNAMIC MODEL AND GEOMETRY DEFINITIONS

The hydrodynamic model describes the discharge plasma as the collective motion of electrons, positive ions, and negative ions. This model incorporates three continuity partial differential equations (PDEs)-including the dynamics and interactions of charged particles and development of space charge—strongly coupled with Poisson's equation—accounting for the mutual influence of space charge and interelectrode electric field. In addition, the secondary electron emission flux resulting from the impact of positive ions on the cathode surface—widely acknowledged as the primary mechanism sustaining negative discharges—is incorporated. In this study, we adopted the same set of governing equations, swarm parameters, initial and boundary conditions, and the stabilization technique as described in our earlier publication [13]. In order to calculate the time-varying current resulting from the motion of charged particles between two electrodes, Sato's equation is used [21]. In this paper, the numerical simulations follow a structured approach such that a validated base case is implemented as a benchmark, offering the reference results against which other cases are compared. Subsequent cases are specifically designed to evaluate how sensitive and responsive are the simulation outputs to variations in cathode geometries, employing different approximations compared to the one defined in the base case. To ensure accuracy, a fine mesh with a resolution of 1 µm is employed for

a circular region centered at the needle tip, with a radius of 0.1 mm, in all cases. The cathode needle is subjected to a -5.5 kV DC voltage in every case. All simulations are conducted using a 2D-axisymmetric model, employing r-z coordinates.

The computational domain for each case is confined by artificial boundaries located 10 mm away from the grounded plane at the top and the needle tip at the sides. Additionally, all needle cathodes are positioned at a distance of 3.3 mm from the grounded plane, which is situated at z = 0. The base case involves a hyperboloid-shaped needle with a radius of curvature of 250 µm. The choice of this configuration is motivated by its utilization and validation in [14] as well as various other documented research endeavors. The geometry in this case is defined by the equation of the upper branch of a vertical hyperbola, centered at the origin with a radius of curvature of 250 µm, i.e., $z = \sqrt{3.3^2 + 13.2r^2}$ (in mm). For the 2nd to 4th cases, three vertical ellipses are introduced, each having the same radius of curvature but varying in terms of their axis lengths. The radius of curvature of 250 µm corresponds to an equation of $a^2 = 0.25b$, where (a, b) represents the semiminor and semi-major axes of the ellipses; specifically, the ellipses are characterized by the following axes lengths: (1.118, 5), (1.581, 10), and (5, 100) (in mm). The 5th and 6th geometries are formed by incorporating a circle with a radius of 250 μm, along with two tangents. The tangents are drawn from the circle to specific points at the top artificial boundary, namely (± 3.5 , 10) and $(\pm 4.5, 10)$ (in mm), respectively. To differentiate between the different cases analyzed in this study, they are denoted as C1, C2, C3, C4, C5, and C6 in both the figures and the corresponding textual descriptions. Fig. 1 showcases the axisymmetric half-geometries of these cases, along with the corresponding initial (t = 0 s) electric potential and electric field distribution. From this figure, it is evident that C2 and C6 elliptic represent extreme and circle-with-tangents configurations; in the former, the major semi-axis is smaller than the distance from the needle tip to the upper open boundary, resulting in the formation of an additional obtuse angle, while the latter has an uncommonly wide shape.

III. NUMERICAL STUDY: A COMPARATIVE ANALYSIS

This section presents a detailed comparative analysis of numerical simulations, evaluating discharge current, spatiotemporal evolution of charged particles, and electric field distribution across all mentioned cases. Fig. 2 illustrates the time variation of the discharge current and the first Trichel pulse for the considered configurations. As anticipated, the extreme cases of C2 and C6 demonstrate the maximum and minimum peak values of discharge current, observed at the earliest and

latest instances, respectively. The other two elliptic needles, C3 and C4, exhibit higher peak values of the pulse compared to the hyperbolic needle, C1. To provide a clearer comparison, the peak value of the first pulse in the elliptic needles of C3 and C4 is 40% and 32% higher than that of the hyperbolic needle, respectively. Additionally, these peak values occur at an earlier time compared to the base case, indicating a higher frequency of the Trichel pulse train. On the other hand, the needle configurations formed from a circle and tangents demonstrate a wider range of results. Specifically, in C5, the pulses occur at higher magnitudes and frequencies compared to the base case, while in C6, characterized by a wider needle, these quantities are lower than those of the base case.

This arrangement for discharge current in different cases aligns with and can be attributed to the evolution of space charge. To gain deeper insight into the behavior of plasmas under various geometries, the following analysis provides a detailed discussion on the initiation and propagation of discharges, focusing on the spatiotemporal variations in the concentrations of charged particles. Figs. 3, 4, and 5 illustrate the concentration of three generic types of charged species, i.e., electrons, positive ions, and negative ions for all cases. The graphs for each case present data for two time instances, corresponding to 10% of the peak discharge current values (represented by solid lines) and the peak discharge current values (represented by dashed lines). These graphs specifically focus on the discharge activities occurring within the ionization regions along a perpendicular arc of 0.2 mm in length starting from the needle tip, which serves as the origin of the graphs, and extending toward the grounded plane.

When the negative DC high voltage is applied to the needle, the initial positive ions are drawn toward the needle due to the electrostatic attraction, while the initial electrons are repelled and directed toward the grounded plane. Within the first few nanoseconds, as the electrons quickly drift away, their rate of ionizing collisions with neutral molecules decreases while the distance from the needle increases. Subsequently, the focal point of ionization activity shifts back to the vicinity of the needle and remains concentrated there until the number density of electrons and positive ions reaches the critical threshold—on the order of 10²⁰ m⁻³—for the formation of the first Trichel pulse. This pre-pulse period is characterized by an electric field that is solely derived from the applied external voltage and has not yet been influenced by space charge distortions.

The time at which the discharge current reaches approximately 10% of its peak value corresponds to the initial stage of pulse rising, where the electron and positive ion concentrations have reached the critical level for the subsequent

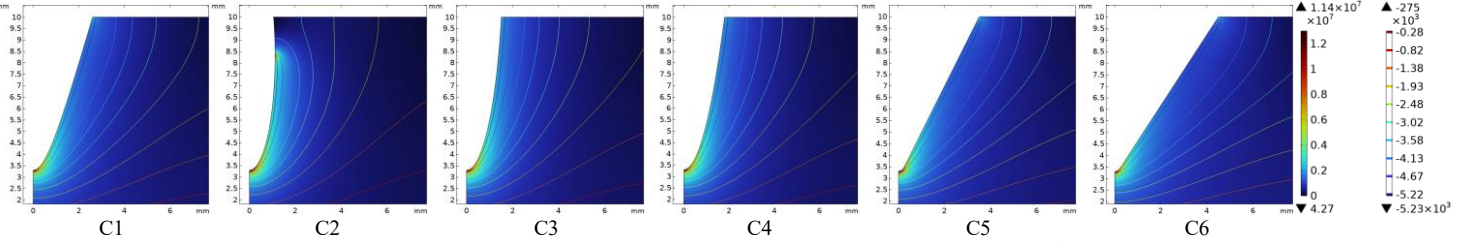


Fig. 1. Axisymmetric half-geometries of needle electrodes with initial distributions of electric field (surface), V·m¹, and electric potential (contour), V.

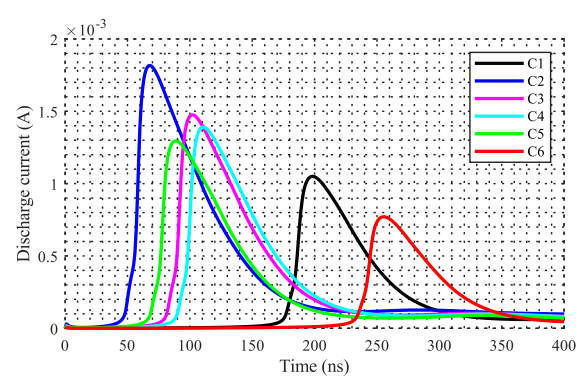


Fig. 2. Interelectrode discharge current: the first Trichel pulse.

rapid increase, occurring within a time frame of around thirty to forty nanoseconds. Concurrently, the main ionization activities maximally shift toward the cathode, accompanied by an exponential growth in the number density of charged particles, as depicted in Figs. 3 and 4. It is important to highlight that there is a strong correlation between the concentration of positive ions and the rate of secondary electron emission, which serves as the predominant mechanism for sustaining the negative discharge. These processes cause a significant distortion in the overall electric field, characterized by a notable increase in proximity to the cathode and a subsequent formation of a dense plasma sheath bordering the cathode surface, within which the electric field approaches zero. This progression coincides with a rapid surge in the current and the initiation of the first Trichel pulse, as evident from Fig. 2.

The time required to reach the critical concentration and the corresponding distance from the needle for maximum ionization activity vary depending on the specific geometry employed. As indicated by the legends in the figures, the chronological sequence for achieving critical concentration and the formation of the first pulse follows the order of C2, C5, C3, C4, C1, and C6. As previously mentioned, this implies a lower pulse train frequency for the hyperbolic needle in comparison to elliptic needles with the same radius of curvature. However, this trend does not apply universally to geometries formed from a circle (with the same radius) with tangents. Furthermore, the number densities of particles do not necessarily align with this temporal order. For instance, the elliptic cathode in C3 exhibits a higher concentration of electrons and positive ions compared to the narrower circle-with-tangents geometry in C5. For C5 and C1, the initiation of pulse rising is characterized by a focal point of ionization activities that is relatively closer to the cathode. However, at the peak of the current pulse, the focal point for ionization activities in elliptic needles shifts closest to the needle tip, with the spatial order directly correlated to their semi-axis length. This results in the formation of a denser plasma within a smaller volume near the tips of elliptic needles. In contrast, circle-with-tangents geometries exhibit a focal point for ionization activities that is relatively farther away at the time corresponding to the maximum current.

In parallel to the evolution of electrons and positive ions, the behavior of negative ions also plays a significant role in the overall dynamics of the discharge. Upon application of the negative DC high voltage, electrons decelerate as they drift

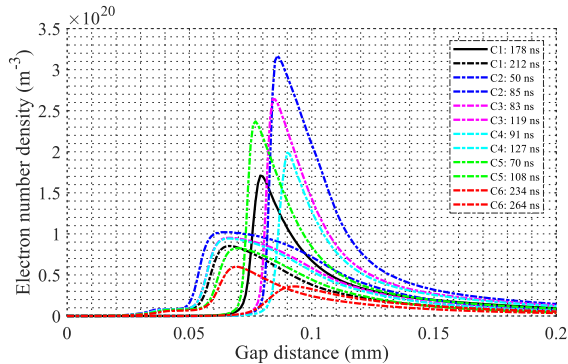


Fig. 3. Electron number density along the symmetry axis

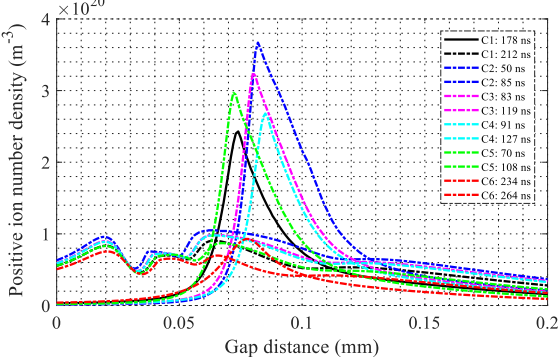


Fig. 4. Positive ion number density along the symmetry axis.

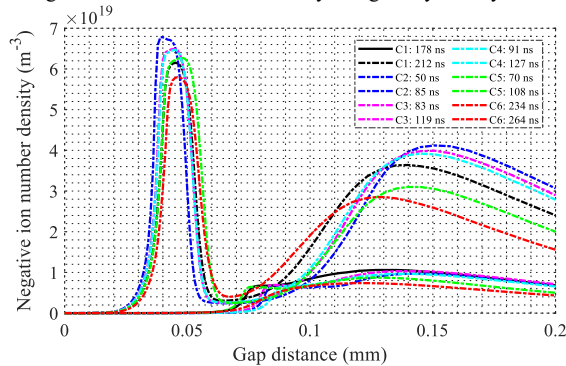


Fig. 5. Negative ion number density along the symmetry axis.

away under the exerted force. In the meantime, electronegative oxygen molecules present in the surrounding air absorb these electrons at a slower rate, leading to the formation of negative ions in front of the avalanche. Initially, during the first few nanoseconds, the attachment activities occur at a decreasing rate and increasing distance from the needle tip, following a pattern similar to the ionization process. However, after a brief period, the focal point of attachment activity shifts closer to the cathode, exhibiting an exponential growth rate until the current pulse formation. As a consequence of electron attachment, the formation of a negative space charge enveloping the ionization region causes a significant reduction in the electric field strength below the critical level needed to sustain the avalanche, leading to a prompt suppression of the avalanche development. As the electrons and positive ions approach the critical concentration necessary to trigger the pulsation of the discharge current and the ionization wave advances toward the cathode, the attachment activities, under their influence, further migrate toward the cathode and continue to exhibit exponential growth.

As shown in Fig. 5, at the time corresponding to the discharge current being 10% of its peak value, the ionization activities in C5 and C1 are relatively closer to the cathode. In contrast to electrons and positive ions, the concentration of negative ions increases during the rise of the current pulse, although at a rate one order of magnitude lower than that of electrons and positive ions. At the peak of the pulse, elliptic needles exhibit more pronounced attachment activities compared to other cases, with their respective focal points being relatively closer to the cathode. This behavior is influenced by the formation of a denser plasma sheath around the elliptic needles, resulting in a spatial concentration of attachment activities in the border region of the ionization area.

The decay of the discharge current pulse coincides with a decrease in the concentration of electrons and positive ions. Simultaneously, the maximum ionization activity region moves away from the cathode, resulting in the expansion of the volume occupied by electrons and positive ions. However, the attachment rate during and even a while after the pulse decay remains high within the drift region—surrounding the expanding ionization region. This leads to a significantly higher density of negative ions compared to electrons and reaching the same order of magnitude or even surpassing the positive charge density. As space charges gradually move away from the needle tip, the distortion in the electric field distribution diminishes, and it tends to revert to its initial distribution. The next Trichel pulse occurs when the negative space charge has cleared a sufficient distance toward the anode, and this pulsating behavior of the interelectrode current repeats.

IV. CONCLUSION

The influence of needle electrode geometry on the behavior of gas discharge plasmas is investigated in this paper. A comprehensive comparative analysis is presented, investigating the initiation and propagation of negative air discharges under different needle shapes with the same radius of curvature. The findings of this study highlight the significance of considering not only the radius of curvature but also the overall geometry and the location of open artificial boundaries in simulation of needle-plane electrode systems. The simulations demonstrated that elliptic needles can generate denser plasmas with increased magnitude and frequency of Trichel pulses compared to needles. Additionally, hyperbolic circle-with-tangents geometries exhibited diverse discharge characteristics, with the tangents angle playing a crucial role. Simultaneously, we have undertaken parallel research efforts, delving deeper into the impact of needle cathode geometry on negative corona discharges, as evidenced by our submitted extended papers [22, 23]. These results emphasize the importance of accurately defining the needle geometry to understand and predict the behavior of gas discharges in electrode systems.

ACKNOWLEDGMENT

This work was supported in part by the U.S. DOE Office of Science, Award DE-SC0021993, and in part by NSF, Award #2306093.

REFERENCES

- M. Ghassemi, A. Barzkar, and M. Saghafi "All-electric NASA N3-X aircraft electric power systems," *IEEE Trans. on Transp. Electrific.*, vol. 8, no. 4, pp. 4091-4104, Dec. 2022.
- [2] A. Barzkar and M. Ghassemi, "Components of electrical power systems in more and all-electric aircraft: A review," *IEEE Trans. on Transp. Electrific.*, vol. 8, no. 4, pp. 4037-4053, Dec. 2022.
- [3] M. Borghei and M. Ghassemi, "A finite element analysis model for partial discharges in silicone gel under a high slew rate, high-frequency square wave voltage in low-pressure conditions," *Energies*, vol. 13, no. 9, p. 2152, May 2020.
- [4] M. Borghei and M. Ghassemi, "Investigation of low-pressure condition impact on partial discharge in micro-voids using finite-element analysis," *IEEE Energy Convers. Congr. & Expo.*, 2020, pp. 3293-3298.
- [5] A. Azizi and M. Ghassemi, "Design of high power density MVDC cables for wide body all electric aircraft," *IEEE Trans. Dielectr. Electr. Insul.*, Early Access, 2023, doi: 10.1109/TDEI.2023.3285849.
- [6] A. Azizi, M. Ghassemi, and J. M. Lehr, "Heat transfer challenges for MVDC power cables used in wide body all electric aircraft under low pressures," *IEEE Access*, vol. 10, pp. 111811–111819, 2022.
- [7] A. Azizi, M. Ghassemi, and J. Lehr, "Design of a cable system for a highpower density MVDC aircraft electric power system," *IEEE Conf. Electrical Insul. Dielectric Phenomena (CEIDP)*, 2022, pp. 151-154.
- [8] A. Azizi, A. Saha, and M. Ghassemi, "A cuboid geometry design for MVDC power cables for using in future all electric wide body aircraft," *IEEE Conf. Electr. Insul. Dielectr. Phenomena (CEIDP)*, 2023.
- [9] A. Saha, A. Azizi, and M. Ghassemi, "An optimal bipolar MVDC coaxial power cable design for envisaged all electric wide body aircraft," *IEEE Conf. Electrical Insul. Dielectric Phenomena (CEIDP)*, 2023.
- [10] M. Ghassemi, "High power density technologies for large generators and motors for marine applications with focus on electrical insulation challenges," *IET High Voltage*, vol. 5, no. 1, pp. 7-14, Feb. 2020.
- [11] G. W. Trichel, "The mechanism of the negative point to plane corona near onset," *Phys. Rev.*, vol. 54, no. 12, pp. 1078–1084, 1938.
- [12] W. L. Lama and C. F. Gallo, "Systematic study of the electrical characteristics of the "Trichel" current pulses from negative needle-toplane coronas," *J. Appl. Phys.*, vol. 45, no. 1, pp. 103–113, 1974.
- [13] M. Hamidieh and M. Ghassemi, "Simulation and analysis of initial stages of negative discharges in air for needle-plane electrode configuration," *IEEE Int. Power Modulator and High Voltage Conf. (IPMHVC)*, Knoxville, TN, USA, 2022, pp. 120–123.
- [14] T. N. Tran, I. O. Golosnoy, P. L. Lewin, and G. E. Georghiou, "Numerical modelling of negative discharges in air with experimental validation," *J.* of Phys. D: Appl. Phys., vol. 44, no. 1, p. 015203, 2010.
- [15] P. Sattari, G. S. P. Castle, and K. Adamiak, "Numerical simulation of Trichel pulses in a negative corona discharge in air," *IEEE Trans. Industry Appl.*, vol. 47, no. 4, pp. 1935–1943, 2011.
- [16] X. Meng, H. Song, G. Sheng, and X. Jiang, "Experimental and simulation study on luminous characteristics of Trichel discharge in air at picosecond time resolution," *High Voltage*, pp. 1–12, 2022.
- [17] Z. Sun, Z. K. Shao, X. Sun, and W. F. Sun, "Trichel pulse characteristics and mechanism of negative corona discharge in sub-millimeter gaps," *Phys. Plasmas*, vol. 30, no. 6, 2023.
- [18] Yu. S. Akishev, I. V. Kochetov, A. I. Loboiko, and A. P. Napartovich, "Numerical simulations of Trichel pulses in a negative corona in air," *Plasma Phys. Reports*, vol. 28, no. 12, pp. 1049–1059, 2002.
- [19] Z. Zhang et al., "Microscopic analysis of Trichel's pulse characteristics and the effect of air pressure and temperature," *Phys. Plasmas*, vol. 29, no. 12, p. 123902, 2022.
- [20] A. O. Kokovin, A. V. Kozyrev, and V. Y. Kozhevnikov, "Simulation of negative corona discharge in atmospheric air: From mode of trichel pulses to stationary discharge," *J. Phys.: Conf. Ser.*, vol. 2064, p. 012024, 2021.
- [21] R. Morrow and N. Sato, "The discharge current induced by the motion of charged particles in time-dependent electric fields; Sato's equation extended," J. Phys. D, Appl. Phys., vol. 32, no. 5, 1999.
- [22] M. Hamidieh and M. Ghassemi, "Impact of cathode geometry on negative corona discharge and Trichel pulse characteristics: A comparative analysis of hyperbolic, elliptic, and tangent-circular needle shapes," *IEEE Trans. Plasma Sci.*, submitted for publication.
- [23] M. Hamidieh and M. Ghassemi, "Conic cross-sectional electrodes and their influence on negative corona discharge and Trichel pulse characteristics," *J. Phys. D, Appl. Phys.*, submitted for publication.